

Large-scale semi-discrete optimal transport with distributed Voronoi diagrams

Bruno Lévy

Inria Saclay, Université Paris Saclay, CNRS, Labo. de Maths. d'Orsay

`Bruno.Levy@inria.fr`

May the 4th, 2024

Abstract

In this article, I propose a numerical method to solve semi-discrete optimal transport problems for gigantic pointsets (10^8 points and more). By pushing the limits by several orders of magnitude, it opens the path to new applications in cosmology, fluid simulation and data science to name but a few. The method is based on a new algorithm that computes (generalized) Voronoi diagrams in parallel and in a distributed way. First I make the simple observation that the cells defined by a subgraph of the Delaunay graph contain the Voronoi cells, and that one can deduce the missing edges from the intersections between those cells. Based on this observation, I introduce the Distributed Voronoi Diagram algorithm (DVD) that can be used on a cluster and that exchanges vertices between the nodes as need be. I also report early experimental results, demonstrating that the DVD algorithm has the potential to solve some giga-scale semi-discrete optimal transport problems encountered in computational cosmology.

1 Introduction and previous work

1.1 Optimal transport in computational physics

Optimal transport studies displacements that minimize a total integrated transport cost¹, while satisfying a mass conservation constraint. It was initially studied by Gaspard Monge, before the french revolution [Mon84]. A quantum leap in understanding the structure of the problem was made in the 90's by Brenier, with his celebrated polar factorization theorem [Bre91], that revealed rich connections with other fields of mathematics and physics (see [Vil03, Vil09, San15] and references herein). By defining a 'transport distance' (the Wasserstein distance), optimal transport makes it possible to compare a wide variety of objects (shapes, functions, ...). This feature is exploited in many recent works in data science and artificial intelligence. Motivated by the wide spectrum of possible

¹for instance, in L_2 transport, integrated squared distance weighted by transported mass.

application, numerical methods were developed for efficiently computing the optimal transport [PC19, MT20, LS18].

In physics, optimal transport has interesting connections with the least action principle [BB00] and gradient flows [JKO98]. These connections were explored to design new modelling, simulation and inverse methods in fluid simulation [GM18, dGWH⁺15, Lév22, QLdGJ22], cosmological reconstruction [BFH⁺03, FMMS02, LMv21, vLM22, NSLM22, NPL⁺23], alternative theories of gravity [Bre15, LBM24], crowd dynamics [BC13, BCMO16, LMSS20] and climatology [CP84] to name but a few. However, all these methods depend on an efficient way of solving the underlying equation, that is, the Monge-Ampère equation, which may be thought-of as a non-linear generalization of the Poisson equation and that is especially difficult to solve. The Fast Fourier transform had a tremendous impact by making it computationally easy to solve the Poisson equation. Is it possible to find an efficient and scalable computational method that would play the same role for the Monge-Ampère equation and optimal transport ?

A possible candidate is the "entropic regularization" idea [Cut13], that uses a softened iterative projection method in dual space, leading to spectacularly efficient solvers (see [PC19] for a survey). To enable scaling up to problems of very large size, recent works also explore ways of distributing computations, such as multiple domain decomposition [MS24, MFF⁺17]. In the application domain targeted by the present work, that is, computational cosmology, one needs to solve optimal transport problems between the initial condition of the Universe, considered to be uniform², modeled as the Lebesgue measure, and an empirical probability measure, with 10^8 to 10^{10} weighted Dirac masses, where each weighted Dirac mass corresponds to a galaxy cluster, modeled as a punctual mass, which makes sense at the cosmological scale. There are huge variations of density, typically 5 orders of magnitudes or more: there are zones where matter clustered a lot, creating highly dense clusters of galaxies, and other zones nearly completely empty of matter (see Figure 4 P. 19). This makes entropy-regularized methods difficult to use, because they depend on regular grids, and the cell size is conditioned by the shortest distance between two Dirac masses, which would require in our case extremely fine grid resolution, making space requirement and computation time prohibitive³.

To keep the accuracy required to represent these highly heterogeneous distributions of matter, it is possible to use the so called *semi-discrete* optimal transport [Mér11, KMT19, Lév15]. Semi-discrete optimal transport exploits the generality of optimal transport theory, that is written in a very general mathematical language (measure theory), that characterizes not only functions, but also much more irregular objects, such as weighted pointsets (modeled as empirical probability measures). Remarkably, the very same mathematical language can be used from the mathematical modeling to computer implementa-

²it is supposed that the Universe had a uniform density at its early ages, which seems to be confirmed by the cosmic microwave background that is very homogeneous

³but it may be possible to develop a version working with adaptively subdivided grids.

tion, without having mathematical details "lost in translation", as summarized in the next subsection.

1.2 From Monge's problem to semi-discrete OT

Monge's problem Given a set X (for instance a subset of \mathbb{R}^d for some dimension d) and two probability measures μ and ν supported by X , such that $\int_X d\mu = \int_X d\nu$, Monge's problem⁴ introduced in [Mon84] consists in finding a transport map $T : X \rightarrow X$ that minimizes the transport cost:

$$\inf_T \left[\int_X \|T(\mathbf{x}) - \mathbf{x}\|^2 d\mu \right] \quad \text{s.t.} \quad \int_{T^{-1}(B)} d\mu = \int_B d\nu \quad \forall B \text{ borel set } \subset X$$

where the constraint ensures that T is a transport map (that is, any measurable subset B of X contains the same mass as its pre-image through T). If the constraint is satisfied, then one says that ν is the *push-forward* of μ under T , noted $\nu = T\#\mu$.

Kantorovich's relaxation It is interesting to consider a relaxation of Monge's problem above, proposed by Kantorovich in the 40's, that writes:

$$\inf_{\gamma} \left[\int_{X \times X} \|\mathbf{x} - \mathbf{y}\|^2 d\gamma \right] \quad \text{subject to:} \quad \begin{cases} \Pi_1\#\gamma = \mu \\ \Pi_2\#\gamma = \nu \end{cases} \quad (1)$$

In a certain sense, the measure γ to be found, supported by the cartesian product $X \times X$, may be thought of as the "graph of T ", and " $\gamma(\mathbf{x}, \mathbf{y})$ "⁵ may be thought of as how much mass goes from \mathbf{x} to \mathbf{y} . The two constraints ensure that the sum of everything that comes out of \mathbf{x} corresponds to " $\mu(\mathbf{x})$ " and the sum of everything that goes to \mathbf{y} corresponds to " $\nu(\mathbf{y})$ ". The two constraints are written in terms of γ pushed-forward by the projections Π_1 and Π_2 (marginals of γ). A measure γ that satisfies these two marginal constraints is called a *transport plan*.

This relaxed problem is interesting, because the objective function and the constraints in Equation 1 are both linear in the unknown transport plan γ (hence we have a linearly constrained linear problem).

Kantorovich dual and c-transform The linear and linearly constrained nature of Kantorovich's problem calls for taking a look at the dual formulation, that writes:

$$\begin{aligned} & \sup_{\phi, \psi} \left[\int_X \phi(\mathbf{x}) d\mu + \int_X \psi(\mathbf{y}) d\nu \right] \\ & \text{subject to: } \phi(\mathbf{x}) + \psi(\mathbf{y}) \leq \|\mathbf{x} - \mathbf{y}\|^2 \quad \forall \mathbf{x}, \mathbf{y} \in X \times X \end{aligned} \quad (2)$$

⁴Written here with modern notations and with the L_2 cost that we use here, whereas it was originally introduced with the L_1 cost.

⁵With quotes because γ is a probability measure that we should integrate over Borel sets. In this paragraph, to help intuition, we pretend that γ, μ, ν are densities.

where ϕ and ψ , the Lagrange multipliers associated with the marginal constraints, are both functions from X to \mathbb{R} . It is interesting to notice that as compared to the primal problem, that depends on an unknown transport plan $\gamma : X \times X \rightarrow \mathbb{R}$, the dual problem depends on two unknown functions $\phi, \psi : X \rightarrow \mathbb{R}$. When they exist, the optimal transport map T and its inverse are then given by:

$$\begin{aligned} T(\mathbf{x}) &= \mathbf{x} - 1/2 \nabla \phi(\mathbf{x}) \\ T^{-1}(\mathbf{y}) &= \mathbf{y} - 1/2 \nabla \psi(\mathbf{y}) \end{aligned} \quad (3)$$

With computer implementation in mind, by considering the dual problem, we have gained a lot: it seems much easier to manipulate two functions $\phi, \psi : X \rightarrow \mathbb{R}$ (for instance, each of them discretized as a vector of N variables, which means $2N$ variables in total) instead of a measure γ supported by $X \times X$ (that may require N^2 variables to be discretized).

In fact, one can do even better: it is easy to prove that if a pair of functions ϕ, ψ that satisfy the constraint exist, one can further optimize the cost by replacing one of them (say ϕ) with the Legendre-Fenchel transform ψ^c of the other one (in terms of computer implementation, we gain another N variables). Then the dual problem becomes the following optimization problem, that depends on a single function $\psi : X \rightarrow \mathbb{R}$:

$$\begin{aligned} \sup_{\psi} [K(\psi) &= \int_X \psi^c(\mathbf{x}) d\mu + \int_X \psi(\mathbf{y}) d\nu] \\ \text{where: } \psi^c(\mathbf{x}) &= \inf_{\mathbf{x}' \in X} [\|\mathbf{x} - \mathbf{x}'\|^2 - \psi(\mathbf{x}')] \end{aligned} \quad (4)$$

Semi-discrete optimal transport Up to now we did not make any assumption regarding the measures μ and ν (except of course that they have the same total mass). Semi-discrete optimal transport is a special case, where μ is the Lebesgue measure and $\nu = \sum_{i=1}^N \nu_i \delta_{\mathbf{x}_i}$; $\sum_i \nu_i = \int_X d\mu$ is an empirical measure (weighted sum of Dirac masses). In this very particular setting, the Kantorovich dual writes:

$$\begin{aligned} K(\psi) &= \int_X \psi^c(\mathbf{x}) d\mathbf{x} + \sum_{i=1}^N \psi(\mathbf{x}_i) \nu_i \\ &= \int_X \inf_{\mathbf{x}' \in X} [\|\mathbf{x} - \mathbf{x}'\|^2 - \psi(\mathbf{x}')] d\mathbf{x} + \sum_i \psi_i \nu_i \\ &= \sum_i \int_{\text{Lag}_i^\psi} (\|\mathbf{x} - \mathbf{x}_i\|^2 - \psi_i) d\mathbf{x} + \sum_i \psi_i \nu_i \end{aligned} \quad (5)$$

where the subsets $\text{Lag}_i^\psi = \{\mathbf{x} \mid \|\mathbf{x} - \mathbf{x}_i\|^2 - \psi_i < \|\mathbf{x} - \mathbf{x}_j\|^2 - \psi_j \quad \forall j \neq i\}$ are called *Laguerre cells*. The set of all Laguerre cells, that is, the minimization diagram of the functions $\|\mathbf{x} - \mathbf{x}_i\|^2 - \psi_i$, is called a *Laguerre diagram*. The last row of Equation 5 is obtained by re-arranging the terms of the integral on the cells of the minimization diagram (the Laguerre cells).

In this setting, the Kantorovich dual K depends on a vector of N values $\psi(\mathbf{x}_i)$, noted ψ_i in what follows. Unlike ψ that is discrete, attached to the \mathbf{x}_i 's, ϕ is continuous and defined on X , but it is defined as the Legendre-Fenchel dual ψ^c of ψ , hence it is also parameterized by the same N numbers (the ψ_i 's).

Using the expression of the optimal transport map in function of the gradient of ϕ (Eq. 3), and recalling that $\phi = \psi^c$ is the Legendre-Fenchel transform of ψ , it is easy to check that the optimal transport map T sends each point \mathbf{x} to the site \mathbf{x}_i of the Laguerre cell it belongs to:

$$\begin{aligned} \forall \mathbf{x} \in \text{Lag}_i^\psi, T(\mathbf{x}) &= \mathbf{x} - 1/2 \nabla \phi(\mathbf{x}) \\ &= \mathbf{x} - 1/2 \nabla \inf_j [\|\mathbf{x} - \mathbf{x}_j\|^2 - \psi_j] \\ &= \mathbf{x} - 1/2 \nabla (\|\mathbf{x} - \mathbf{x}_i\|^2 - \psi_i) \quad (\text{because } \mathbf{x} \in \text{Lag}_i^\psi) \\ &= \mathbf{x}_i \end{aligned}$$

At this point, we have done nothing else than rewriting the generic optimal transport problem in the specific case where μ is the Lebesgue measure and ν is an empirical measure. Let us see now how to compute the optimal transport in practice, that is, how to determine the N unknown parameters ψ_i . The Kantorovich dual that depends on these parameters is concave and C^2 almost everywhere [Lév15, KMT19, L22] and can be maximized using a Newton method:

Algorithm 1. *Semi-discrete optimal transport*

input: a pointset $(\mathbf{x}_i)_{i=1}^N$ and masses $(\nu_i)_{i=1}^N$
output: the Laguerre diagram $\{\text{Lag}_i^\psi\}_{i=1}^N$ such that $|\text{Lag}_i^\psi| = \nu_i \forall i$

- (0) $\psi \leftarrow 0$
- (1) **while** $\|\nabla K\|_\infty < \epsilon$
- (2) **solve for** \mathbf{p} in $[\nabla^2 K \psi] \mathbf{p} = -\nabla K \psi$
- (3) find descent parameter α (see Algorithm 2)
- (4) $\psi \leftarrow \psi + \alpha \mathbf{p}$
- (5) **end while**

In step (3), the coefficients of the gradient $\nabla K \psi$ and the Hessian $\nabla^2 K \psi$ are given by (derivations in [KMT19]):

$$\begin{aligned} \frac{\partial K}{\partial \psi_i} &= \nu_i - |\text{Lag}_i^\psi| \\ \frac{\partial^2 K}{\partial \psi_i \partial \psi_j} &= \frac{1}{2} \frac{|\text{Lag}_{i,j}^\psi|}{\|\mathbf{x}_j - \mathbf{x}_i\|} \quad \text{if } j \neq i \\ \frac{\partial^2 K}{\partial \psi_i^2} &= -\sum_{j \neq i} \frac{\partial^2 K}{\partial \psi_i \partial \psi_j} \end{aligned} \tag{6}$$

where $|\text{Lag}_{i,j}^\psi|$ denotes the area of the facet common to cells Lag_i^ψ and Lag_j^ψ , or 0 if there is no such facet.

In step (4), a good descent parameter α is found by the provably convergent KMT algorithm [KMT19], as follows:

Algorithm 2. *Kitagawa-Méridot-Thibert descent (KMT)*

input: current values of $(\psi_i)_{i=1}^N$ and Newton direction \mathbf{p}
output: descent parameter α determining the next iterate $\psi \leftarrow \psi + \alpha\mathbf{p}$

(1) $\alpha \leftarrow 1$
(2) **loop**
(3) **if** $\inf_i |\text{Lag}_i^{\psi+\alpha\mathbf{p}}| > a_0$ **and** $\|\nabla K(\psi + \alpha\mathbf{p})\| \leq (1 - \alpha/2)\|\nabla K(\psi)\|$
(4) **then exit loop**
(5) $\alpha \leftarrow \alpha/2$
(6) Compute the Laguerre diagram $(\text{Lag}_i^{\psi+\alpha\mathbf{p}})_{i=1}^N$
(7) **end loop**
 where $a_0 = \frac{1}{2} \min \left(\inf_i |\text{Lag}_i^{\psi=0}|, \inf_i (\nu_i) \right)$.

The KMT algorithm iteratively halves the descent parameter α until two criteria are met: the volume of the smallest cell needs to be larger than a threshold a_0 (first condition in line 3), and the norm of the gradient needs to decrease sufficiently (second condition in line 3). The threshold a_0 for the minimum cell volume corresponds to (half) the minimum cell volume for $\psi = 0$ (also called Voronoi diagram) and minimum prescribed area ν_i .

In the numerical algorithm for semi-discrete optimal transport above, the main two costly operations are computing Laguerre diagrams and solving linear systems. By examining the coefficients of the linear system given in Equation 6, one can notice its similarity with a Poisson system discretized with \mathbb{P}_1 elements on a tetrahedral grid. For such systems, an algebraic multigrid method [Dem19] is highly effective, as we noticed in [LBM24] and confirmed experimentally. In this setting, the lion's share of the computational cost is the computation of Laguerre diagrams: for a typical reconstruction problem in cosmology, it takes 60% of the computation time (whereas matrix assembly and linear solve take 25% and 15% respectively). Besides computational cost, another important obstacle to scaling up is the memory cost of the data structure used to store the Laguerre diagrams. Both aspects call for a distributed algorithm, that could run on a cluster. We shall now see standard algorithms to compute (generalized) Voronoi diagrams, then we will see how to derive a distributed version, that can run on a cluster.

1.3 Voronoi diagrams and algorithms to compute them

Voronoi diagrams are ubiquitously used in various domains of computational sciences, including geometry processing, data analysis, machine learning and computational physics to name but a few. The properties of Voronoi diagrams and their various generalizations were studied [Aur91, EM90] and used to derive efficient computational algorithm, see surveys in [BY98, OBSC00]. To efficiently represent a Voronoi diagram in a computer, one can use the dual combinatorial structure, called the Delaunay triangulation. Historically, one of the first

method, proposed in the 70's by Sloan [Slo87], transforms an arbitrary triangulation into the Delaunay triangulation by flipping the edges until all the triangles are valid, that is, such that their circumcircles are empty of any other point. The main widely used algorithm to compute Voronoi diagram was proposed in the 80's, simultaneously by Bowyer and Watson [Bow81, Wat81]. It also operates on the Delaunay triangulation. It inserts the points one by one in the triangulation, and iteratively discards the triangles that violate the empty circumcircle condition and creates new ones, connecting the newly inserted points to the boundary of the zone where triangles were discarded, which is more efficient than flipping edges.

Numerical precision is an important aspect to be considered with uttermost care when implementing these algorithms. The "neuralgic point" is a set of functions, called geometric predicates, that take as argument geometric objects (for instance two points \mathbf{x}_1 and \mathbf{x}_2) and that returns a discrete value (for instance, +1 if \mathbf{x}_1 is above \mathbf{x}_2 , -1 if \mathbf{x}_1 is below \mathbf{x}_2 and 0 if they have the same altitude). In general, these geometric predicates are more complicated, and correspond to the sign of a polynomial in the point's coordinates. The main difficulty is that the floating point numbers manipulated in computers have limited precision. If no care is taken, the computed signs are not exact, and depending on the order of the operations, the predicate may indicate that \mathbf{x}_1 is above \mathbf{x}_2 in one part of the algorithm, and that \mathbf{x}_1 is below \mathbf{x}_2 in another part, leading to incoherencies in the constructed combinatorial structure. For this reason, different techniques were proposed to compute the exact sign of the polynomial, and several software packages were proposed, by Shewchuk [She97] (who uses arithmetic expansions), in CGAL [The23] (that uses a combination of arithmetic filters, interval arithmetic and exact numbers), PCK [Lév16] and GEOGRAM [Inr23], that use a combination of arithmetic filters and arithmetic expansions.

To speed-up the computation of Voronoi diagrams, a parallel algorithm based on the "security radius" theorem was proposed [LB12], as well as a version that runs on GPUs for Voronoi and Laguerre diagrams [RSL18, BAR⁺21]. To compute Delaunay triangulations and Voronoi diagram with gigantic pointsets, several techniques were proposed, based on decomposing the input domain into regions. The "streaming" algorithm proposed in [ILSS06] inputs a stream of points and outputs a stream of triangles. It minimizes the globally stored information based on "finalization" tags inserted in the point stream, indicating that a point is the last one in its region, which allows to discard the information that is no-longer needed. Another approach consists in first computing the Delaunay triangulation in each region independently, then determine the points that should be exchanged with the neighboring regions in order to get the correct triangulation / Voronoi cells [PMP14]. I mention also the AREPO code [Spr10], used for large scale cosmological simulations, that is based on a variant of Sloan's edge flipping algorithm, distributed over a cluster, using an algorithm similar to the one in [PMP14]. As done in [CMYB19], a similar result can be obtained by using the *star splaying* algorithm [She05], that can restore the Delaunay

condition in a nearly-Delaunay triangulation. It represents a mesh as a collection of (possibly incoherent) vertex stars, and restores coherency between them.

As explained later, the method proposed in this article shares some similarities with the *stars splaying* idea. The main difference is the path of reasoning that I followed, that is nearly equivalent, but that is structured around the Voronoi cells (instead of the 1-ring neighborhoods). This path of reasoning naturally leads to several algorithms for parallel and distributed Voronoi diagrams. As far as the distributed algorithm is concerned, the approach results in a smaller number of points exchanged between the regions.

With the goal of making it possible for semi-discrete optimal transport (see Section 3) to scale up beyond 10^8 particles, what follows introduces new algorithms to compute (generalized) Voronoi diagrams in parallel and in a distributed way. The idea is based on the simple observation that the cells defined by a subgraph of the Delaunay graph contain the Voronoi cells, and that their intersections define the edges of the Delaunay graph (Section 2.1). From this observation, we deduce two algorithms, a parallel one (PVD for Parallel Voronoi Diagram), described in Section 2.2, that can be used in multicore shared memory machines, and a distributed one (DVD for Distributed Voronoi Diagram), described in Section 2.3, that computes a (potentially gigantic) Voronoi diagram on a cluster, and exchanges vertices between the nodes as need be. The distributed Voronoi Diagram algorithm (DVD) can be used to design a giga-scale semi-discrete optimal transport algorithm (see Section 3 for early results).

2 Distributed Voronoi Diagram

2.1 The Voronoi diagram and the Delaunay graph

We consider a set \mathbf{X} of N points $(\mathbf{x}_i)_{i=1}^N$ in \mathbb{R}^d , and a family of N continuous functions $F_i : \mathbb{R}^d \rightarrow \mathbb{R}$.

Definition 1. *The minimization diagram (also called lower envelope, or generalized Voronoi diagram) [Aur91] is defined as the set of cells $\{\mathcal{V}or_i\}_{i=1}^N$ (called generalized Voronoi cells):*

$$\mathcal{V}or_i = \{\mathbf{x} \mid F_i(\mathbf{x}) < F_j(\mathbf{x}) \quad \forall j \neq i\}.$$

Examples

- If $F_i(\mathbf{x}) = \|\mathbf{x} - \mathbf{x}_i\|^2$, then the minimization diagram is called a *Voronoi diagram*;
- if $F_i(\mathbf{x}) = \|\mathbf{x} - \mathbf{x}_i\|^2 - \psi_i$ for a vector of N scalars ψ_i , then the minimization diagram is called a *Laguerre diagram* (or power diagram).

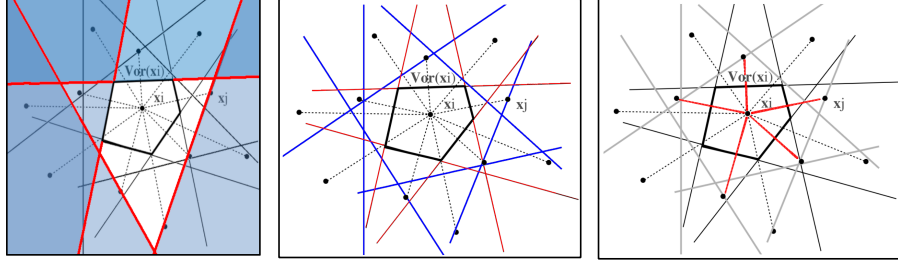


Figure 1: Left: the intersection of four half-spaces $\Pi^+(i, j)$ (their boundaries are highlighted in red). The area shaded in blue corresponds to the excluded half-spaces. The white region corresponds to the intersection between four half-spaces. It contains the Voronoi cell. Center: The Voronoi cell $\mathcal{V}or(\mathbf{x}_i)$ corresponds to the intersection of all the half-spaces $\Pi^+(i, j)$. Among them, some touch the boundary of $\mathcal{V}or(\mathbf{x}_i)$ and are contributing (in red), and some are non-contributing (in blue). Right: the Delaunay graph (in red) corresponds to the set of edges $(i - j)$ such that $\Pi^+(i, j)$ is contributing to $\mathcal{V}or(\mathbf{x}_i)$ (or equivalently, $\Pi^+(j, i)$ is contributing to $\mathcal{V}or(\mathbf{x}_j)$).

By definition of the Voronoi cells, as illustrated in Figure 1, one can observe that

$$\mathcal{V}or_i = \bigcap_{j \neq i} \Pi^+(i, j)$$

where the *dominance region* $\Pi^+(i, j)$ is defined by :

$$\Pi^+(i, j) = \{\mathbf{x} \mid F_i(\mathbf{x}) < F_j(\mathbf{x})\}.$$

Consider now a set of oriented edges $\mathcal{E} = \{(i \rightarrow j)\}$ and the regions $\{\mathcal{V}_i^\mathcal{E}\}_{i=1}^N$ defined by:

$$\mathcal{V}_i^\mathcal{E} = \bigcap_{(i \rightarrow j) \in \mathcal{E}} \Pi^+(i, j).$$

One can make the following (trivial yet useful) observation:

Observation 1. *Given an arbitrary set \mathcal{E} of oriented edges, each region $\mathcal{V}_i^\mathcal{E}$ contains the Voronoi cell of point \mathbf{x}_i :*

$$\mathcal{V}or_i \subset \mathcal{V}_i^\mathcal{E} \quad \forall \mathcal{E}, \forall i$$

Proof. This property is directly deduced from the characterization of $\mathcal{V}or_i$ (7) and the definition of $\mathcal{V}_i^\mathcal{E}$ (8). \square

Definition 2. *Given a set of points $\mathbf{X} = \{\mathbf{x}_i\}_{i=1}^N$, the Delaunay graph (or Delaunay skeleton) $\mathcal{D}el(\mathbf{X})$ is the adjacency graph of the Voronoi cells, that is, the set of (non-oriented) edges $(i - j)$ defined by:*

$$\mathcal{D}el(\mathbf{X}) = \{(i - j) \mid \partial \mathcal{V}or_i \cap \partial \mathcal{V}or_j \neq \emptyset\}$$

Our goal is now to find a way of computing the Delaunay graph from an arbitrary oriented graph \mathcal{E} . Note: what we want to compute can be also a *supergraph* of $\mathcal{D}el(\mathbf{X})$ because as soon as all the edges of $\mathcal{D}el(\mathbf{X})$ are included in \mathcal{E} , then each cell $\mathcal{V}_i^\mathcal{E}$ corresponds to the Voronoi cell $\mathcal{V}or_i$:

$$\mathcal{D}el(\mathbf{X}) \subset \mathcal{E} \implies \forall i, \mathcal{V}_i^\mathcal{E} \left(= \bigcap_{j \neq i} \Pi^+(i, j) \right) = \mathcal{V}or_i.$$

The set of points $\Pi(i, j) = \{\mathbf{x} \mid F_i(\mathbf{x}) = F_j(\mathbf{x})\}$ "equidistant" relative to \mathbf{x}_i and \mathbf{x}_j is called a *bisector*. If a bisector $\Pi(i, j)$ has a non-empty intersection with the border $\mathcal{V}or_i$ of a Voronoi cell, then the oriented edge $(i \rightarrow j)$ is said to be *contributing* to the Voronoi cell $\mathcal{V}or_i$, else it is *non-contributing*.

In terms of these definitions, starting from an arbitrary oriented graph \mathcal{E} , our goal is to find a new graph \mathcal{E}' that contains all the contributing oriented edges that are missing in \mathcal{E} . To do so, we make another simple observation:

Observation 2. *Given a pointset \mathbf{X} and an arbitrary oriented graph \mathcal{E} , and given an edge $e = (i - j)$ in the Delaunay graph of \mathbf{X} , either the oriented edges $(i \rightarrow j)$ and $(j \rightarrow i)$ are both in \mathcal{E} , or the cells $\mathcal{V}_i^\mathcal{E}$ and $\mathcal{V}_j^\mathcal{E}$ have a non-empty intersection.*

Proof. Consider an edge of the Delaunay graph $e = (i - j) \in \mathcal{D}el(\mathbf{X})$. The presence of this edge means that the intersection between the border of $\mathcal{V}or_i$ and the border of $\mathcal{V}or_j$ is non-empty. In other words, there exists a point \mathbf{x} in the intersection of $\partial\mathcal{V}or_i$ and $\partial\mathcal{V}or_j$. Then there are two cases:

- the point \mathbf{x} belongs to both the border of $\mathcal{V}_i^\mathcal{E}$ and the border of $\mathcal{V}_j^\mathcal{E}$. Then the edge $e = (i - j)$ is already in \mathcal{E} ;
- or the point \mathbf{x} belongs to the interior of $\mathcal{V}_i^\mathcal{E}$ or to the interior of $\mathcal{V}_j^\mathcal{E}$ (recalling that $\mathcal{V}or_i \subset \mathcal{V}_i^\mathcal{E}$), which implies that $\mathcal{V}_i^\mathcal{E}$ and $\mathcal{V}_j^\mathcal{E}$ have a non-empty intersection.

□

2.2 PVD: Parallel Voronoi Diagram

From Observation 2, one can deduce a new algorithm to compute a Voronoi diagram:

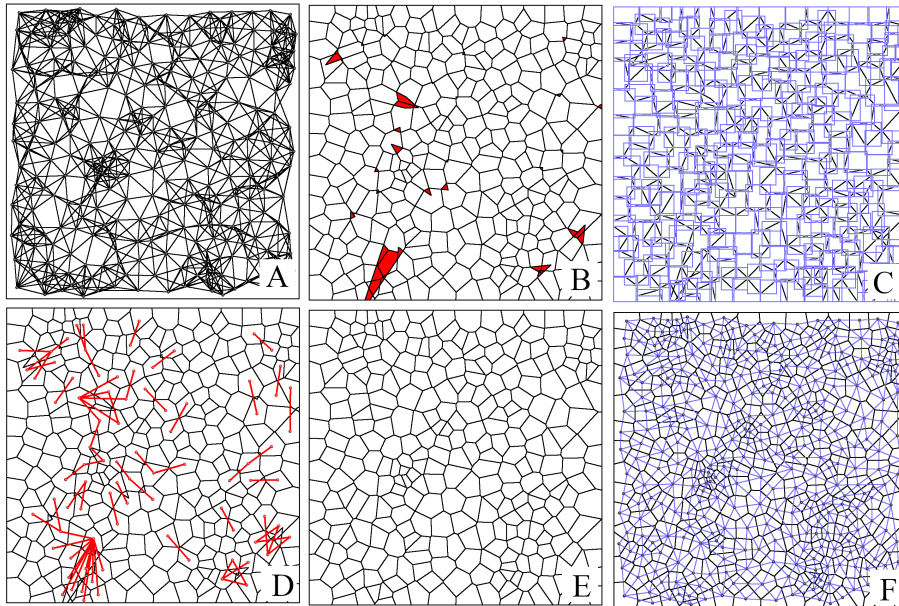


Figure 2: A: k-NN graph; B: the cells deduced from the k-NN graph. They mostly correspond to the Voronoi diagram, except some intersections (in red); C: detecting the intersections with an Axis-Aligned Bounding Box tree; D: adding an edge in the graph for each pair of intersecting cells; E: the cells now correspond to Voronoi cells; F: the Delaunay graph contains the edges that correspond to the contributing bisectors. One gets the Voronoi cells as soon as the graph contains all these edges (as is the case at step D).

Algorithm 3. *Parallel Voronoi Diagram (PVD)*

input: a pointset \mathbf{X}
output: the Voronoi diagram $\{\mathcal{V}or_i\}_{i=1}^N$

- (1) $\mathcal{E} \leftarrow kNN(\mathbf{X})$
- (2) compute the cells $(\mathcal{V}_i^\mathcal{E})_{i=1}^N$
- (3) $\mathcal{E} \leftarrow \mathcal{E} \cup \{(i-j) \mid \mathcal{V}_i^\mathcal{E} \cap \mathcal{V}_j^\mathcal{E} \neq \emptyset\}$
- (4) re-compute the cells $(\mathcal{V}_i^\mathcal{E})_{i=1}^N$

where:

- in step (1), the k-nearest neighbor graph is extracted from a kD-tree (Figure 2-A). Both the kD-tree construction and extraction of the k-nearest neighbors is computed in parallel;
- in step (2), the cells $V_i^\mathcal{E} = \bigcap_{(i \rightarrow j) \in \mathcal{E}} \Pi^+(i, j)$ are computed in parallel. In the case of a Voronoi diagram or Laguerre diagram, the dominance regions $\Pi^+(i, j)$ are half-spaces. Their intersection are efficiently computed by representing the cells in dual form [Aur91, L22]. The cells computed at step (2) are shown in Figure 2-B. As one can see, the set of cells $\mathcal{V}_i^\mathcal{E}$ deduced from the k-NN graph \mathcal{E} is very near the Voronoi diagram, except for a few overlaps between the cells (in red);
- in step (3), we use an axis-aligned bounding box tree to determine a set of candidate intersection pairs (Figure 2-C). Then all the candidate intersections are processed in parallel. Each time the bounding boxes of a pair of cells $\mathcal{V}_i^\mathcal{E}$ and $\mathcal{V}_j^\mathcal{E}$ have an intersection, the edges $(i-j)$ and $(j-i)$ are appended to \mathcal{E} (in red in Figure 2-D). This will insert too many edges, but remember that what we want to compute is a *surgraph* of the Delaunay graph;
- in step (4), each re-computed cell $V_i^\mathcal{E}$ corresponds to the Voronoi cell $\mathcal{V}or_i$ (since $\mathcal{D}el(\mathbf{X}) \subset \mathcal{E}$). The so-computed Voronoi diagram is shown in Figure 2-E. The Delaunay graph is shown in Figure 2-F. All its edges are contained either in the k-NN graph (Figure 2-A) or in the edges coming from cell intersections (Figure 2-D).

The Delaunay triangulation, if needed, is deduced from the combinatorics of the Voronoi diagram. In 3D, a tetrahedron (i, j, k, l) is generated each time the intersection between the dominance regions $\Pi^+(i, j)$, $\Pi^+(i, k)$, $\Pi^+(i, l)$ define a vertex of $\mathcal{V}or_i$. To avoid obtaining the tetrahedra four times, one can keep only the one for which i is the smallest index. To make sure the same tetrahedra are generated from different Voronoi cell, one needs to take care of configurations with cospherical points, that generate Voronoi vertices of degree potentially

larger than 4, hence several possible tetrahedralizations. A simple solution is to use the classical symbolic perturbation approach [EM90]. The only predicate used by the computation of the cells $V_i^{\mathcal{E}}$ requires to classify a Voronoi vertex, that is, the intersection of three bisectors, relative to a fourth bisector, which is equivalent to the `in_sphere` predicate (for Voronoi diagrams), or its weighted generalization (for Laguerre diagrams). Symbolically-perturbed implementations of these predicates are readily available [She97, Lév16, Inr23, The23].

This algorithm is very similar to *star splaying* [She05], that also starts from a subset of the Delaunay graph, and finds the missing edges. In other words, one may describe this algorithm as "star splaying seen from the point of view of the Voronoi cells". It adds an alternative way of considering the neighborhoods, in addition to the three points of view usually associated with star splaying ("star of Delaunay vertex", "convex hull of ray" and "cross-section of cone"). The four points of view are formally equivalent, but focusing on Voronoi cells has three practical consequences:

- it may be a question of taste, but one may find the explanation in terms of Voronoi cells shown in Figure 2 easier to follow: simply put, the dual of "star splaying" is "Voronoi clipping" or "Voronoi trimming";
- instead of storing all the vertex's neighborhoods, one can store only the graph, and recompute the Voronoi cells as need be. While this has an additional computational cost, it saves substantial amounts of memory;
- by considering the Voronoi cells explicitly, one can exploit their relations with the boundary of the domain to optimize point exchanges in the distributed algorithm, as explained in the next section.

2.3 DVD: Distributed Voronoi Diagram

We now suppose that the domain is partitioned into M regions $(R_k)_{k=1}^M$, and that the pointset \mathbf{X} is partitioned accordingly, into M subsets $\mathbf{X}_k = \mathbf{X} \cap R_k$. In addition, we suppose that each region R_k is represented and processed by a different node of a cluster. Each node k is going to exchange some points with other nodes in order to ensure that it obtains all the necessary information to compute all the voronoi cells of the points \mathbf{X}_k .

Algorithm 4. *By-region parallel Voronoi Diagram*

Input: the regions $\{R_k\}_{k=1}^M$ and the pointsets $\{\mathbf{X}_k\}_{k=1}^M$
Output: M graphs \mathcal{E}_k , such that $\mathcal{V}or_i = \mathcal{V}_i^{\mathcal{E}_k} \forall \mathbf{x}_i \in R_k$

- (1) **for** $k = 1 \dots M$, $\mathcal{E}_k \leftarrow \mathcal{D}el(\mathbf{X}_k)$
- (2) **for** $k = 1 \dots M$, $\mathbf{Y}_k \leftarrow \left\{ \mathbf{x}_i \in R_l \mid l \neq k \text{ and } \mathcal{V}_i^{\mathcal{E}_l} \cap R_k \neq \emptyset \right\}$
- (3) **for** $k = 1 \dots M$, $\mathcal{E}_k \leftarrow \mathcal{D}el(\mathbf{X}_k \cup \mathbf{Y}_k)$
- (4) **for** $k = 1 \dots M$, $\mathbf{Z}_k \leftarrow \{ \mathbf{x}_j \mid \exists l \neq k, \exists (i \rightarrow j) \in \mathcal{E}_l, \mathbf{x}_i \in \mathbf{X}_k, \mathbf{x}_j \in \mathbf{X}_l \}$
- (5) **for** $k = 1 \dots M$, $\mathcal{E}_k \leftarrow \mathcal{D}el(\mathbf{X}_k \cup \mathbf{Y}_k \cup \mathbf{Z}_k)$

As in the previous section, in step (1), the algorithm starts by computing a graph \mathcal{E} , but this time the graph is distributed over a set of M nodes, $\mathcal{E} = \mathcal{E}_1 \cap \dots \cap \mathcal{E}_M$, and each component \mathcal{E}_k stored in a node corresponds to the Delaunay graph $\mathcal{D}el(\mathbf{X}_k)$ of the vertices of \mathbf{X} that fall in the region R_k associated with that node. To compute the Delaunay graph, one may use the standard Bowyer-Watson algorithm [Bow81, Wat81], or Algorithm 3 in the previous section. Once the Delaunay graph \mathcal{E}_k is computed, most cells $\mathcal{V}_i^{\mathcal{E}_k}$ correspond to the Voronoi cells $\mathcal{V}or_i$ (since \mathcal{E}_k is the Delaunay graph of \mathbf{X}_k), except for some cells on the boundary, that are larger than the Voronoi cells (Observation 1). The edges $(i - j)$ that are missing in \mathcal{E}_k correspond to pairs of cells with non-empty intersections (Observation 2), stored in different nodes. To have in each \mathcal{E}_k all the edges of the Delaunay graph, we need to determine both the relation i is clipped by j (that corresponds to the oriented edge $(i \rightarrow j)$) and the relation i is clipping j (that corresponds to the oriented edge $(j \rightarrow i)$), hence we have an algorithm that operates in two phases (steps (2,3) and steps (4,5)): in step (2), each node k gathers the points $\mathbf{x}_i \in R_l$ with a cell $\mathcal{V}_i^{\mathcal{E}_l}$ that has a non-empty intersection with R_k (to detect the missed *is clipped by* relations). In step (3), the graphs are updated. In step (4), the so-discovered new edges are symmetrized, by sending back the neighbors (*is clipping* relations). Each graph \mathcal{E}_k obtained in the node k at step (5) has all the edges to properly compute the Voronoi cells of the points in R_k .

Why do we need two steps ? (that is, step (2) and step (4) ?). Our goal is to represent, in a distributed manner, a graph $\mathcal{E} = \bigcup_k \mathcal{E}_k$ that has all the edges of the Delaunay graph $\mathcal{D}el(\mathbf{X})$. For each (unoriented) edge $(i - j) \in \mathcal{D}el(\mathbf{X})$, we need to find the two oriented edges $(i \rightarrow j)$ (that corresponds to the relation *i is clipped by j*) and $(j \rightarrow i)$ (that corresponds to the relation *i is clipping j*) in all the nodes that contain \mathbf{x}_i or \mathbf{x}_j , hence two steps are needed. Let us examine them more closely:

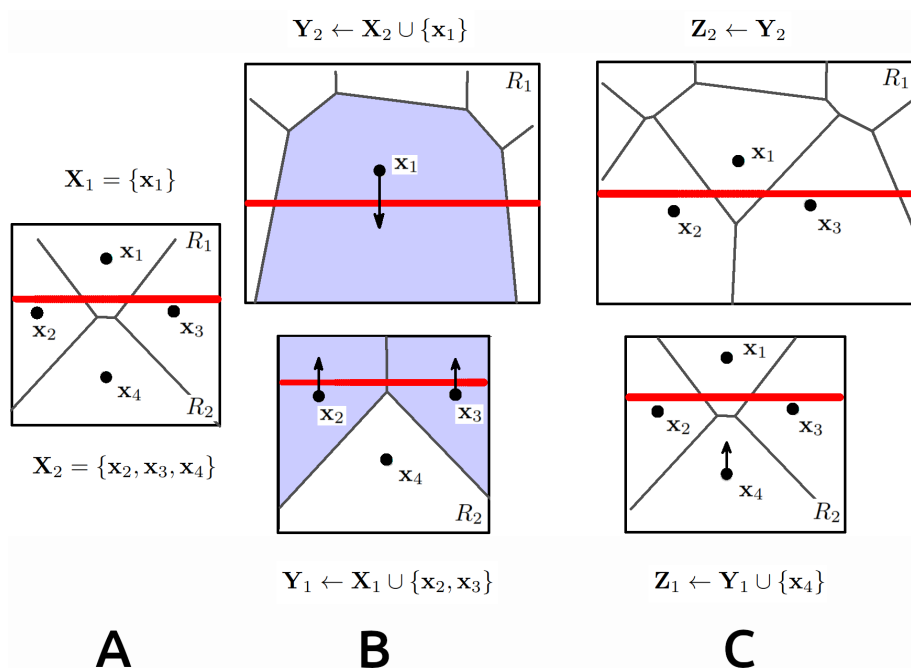


Figure 3: A simple example showing why two steps of point exchange are needed in the distributed Voronoi diagram algorithm.

- Step (2) ensures that for all \mathbf{x}_i in a region R_k , all the edges $(j \rightarrow i)$ such that $(i - j) \in \mathcal{D}el(\mathbf{X})$ are in the $\mathcal{E}_{l, l \neq k}$ (that is, the *i is clipping j* relation, for the x_j 's in the other regions);
- Step (4) ensures that for all \mathbf{x}_i in a region R_k , all the edges $(i \rightarrow j)$ such that $(i - j) \in \mathcal{D}el(\mathbf{X})$ are in \mathcal{E}_k (that is, the *i is clipped by j* relation, for the x_j 's in the other regions).

Hence step (4) is simply a combinatorial operation that *symmetrizes* the oriented edges discovered at step (2).

An example is shown in Figure 3. One wants to compute the Voronoi diagram shown on the left, using two regions R_1 and R_2 . The boundary between R_1 and R_2 is shown in red. The sets of points \mathbf{X}_1 and \mathbf{X}_2 are initialized with the points contained by regions R_1 and R_2 respectively, shown in Fig. 3-A. In the first step (Fig. 3-B),

- Region R_1 contains \mathbf{x}_1 . The cell $\mathcal{V}_1^{\mathcal{E}}$ of \mathbf{x}_1 has an intersection with the boundary, hence \mathbf{x}_1 is sent to R_2 .
- Region R_2 contains $\mathbf{x}_2, \mathbf{x}_3$ and \mathbf{x}_4 . The cells of \mathbf{x}_2 and \mathbf{x}_3 have an intersection with the boundary, and are sent to \mathbb{R}_1 .

In the second step (Fig. 3-C), region R_1 knows $\mathbf{x}_1, \mathbf{x}_2$ and \mathbf{x}_3 . The cell $\mathcal{V}_1^{\mathcal{E}}$ is not correct, because it does not know (yet) its neighbor \mathbf{x}_4 , but the neighboring relation $(1 - 4)$ is known by R_2 , that sends \mathbf{x}_4 to \mathbb{R}_1 .

With this by-region granularity, Algorithm 4 can be implemented in a cluster. All the variables with index k are stored in a specific node of the cluster. The five loops in steps (1)-(5) are executed in parallel, by all the nodes in the cluster. The only inter-node communications are at steps (2) and (4) (plus the initial broadcast and partition of \mathbf{X} into the R_k 's). In algorithm 4, at steps (2) and (4) a node k *gathers* points from potentially all the other nodes. From an implementation point of view, it is more natural to have the nodes interconnected with only the neighboring nodes through communication channels. In this setting, the node that corresponds to region R_k is connected to the nodes of the adjacent regions. During the execution of the algorithm, each node *sends* the points where they are needed. This alternative point of view leads to the following algorithm, executed by each node in parallel (the loops on the nodes k are omitted):

Algorithm 5. *Distributed Voronoi Diagram (algorithm for a node k)*

Input: the regions $\{R_k\}_{k=1}^M$ and the pointsets $\{\mathbf{X}_k\}_{k=1}^M$
Output: M graphs \mathcal{E}_k , such that $\mathcal{V}or_i = \mathcal{V}_i^{\mathcal{E}_k} \forall \mathbf{x}_i \in R_k$

- (1) $\mathcal{E}_k \leftarrow \mathcal{D}el(\mathbf{X}_k)$
- (2) **for each** $\mathbf{x}_i \in \mathbf{X}_k$
- (3) **for each** R_l neighbor of R_k
- (4) **if** $\mathcal{V}_i^{\mathcal{E}_k} \cap R_l \neq \emptyset$ **then** send \mathbf{x}_i to neighbor node l
- (5) $\mathbf{Y}_k \leftarrow$ receive points from neighbor nodes
- (6) **sync**
- (7) $\mathcal{E}_k \leftarrow \mathcal{D}el(\mathbf{X}_k \cup \mathbf{Y}_k)$
- (8) **for each** $(i \rightarrow j) \in \mathcal{E}$
- (9) $l \leftarrow Region(\mathbf{x}_i)$; $m \leftarrow Region(\mathbf{x}_j)$
- (10) **if** $l = k$ **and** $m \neq k$ **then** send \mathbf{x}_j to neighbor node m
- (12) $\mathbf{Z}_k \leftarrow$ receive points from neighbor nodes
- (13) **sync**
- (14) $\mathcal{E}_k \leftarrow \mathcal{D}el(\mathbf{X}_k \cup \mathbf{Y}_k \cup \mathbf{Z}_k)$

where **sync** is a synchronization point for all the threads (one waits there until everybody has reached this point), and where $Region(l)$, $Region(m)$ denote the region that sent l (resp. m) at step (5) (each node keeps track of who sent each point).

Each cluster node k , that represents region R_k is typically connected to nodes corresponding to the regions adjacent to R_k . If regions are bounded by polyhedra, adjacent regions can have a face, an edge or a vertex in common with R_k . Typically, one can use a regular grid, with up to four regions incident to each edge and up to eight regions incident to each vertex. If a candidate Voronoi cell encroaches a facet, then the corresponding point is sent to the region connected to the other side of the facet. If the candidate Voronoi cell encroaches an edge or a vertex, then the point is sent to all the regions incident to the edge or the vertex. Note that in this setting, Algorithm 5 does not work if a cell traverses a region completely. If one wants to support this condition, it can be done by executing the two points exchange steps of the algorithm until each point was sent to all the regions it has a non-empty intersection with.

The algorithm also works for Laguerre diagrams, but one needs to take care: in a Laguerre diagram, the cell of \mathbf{x}_i does not necessarily contain \mathbf{x}_i , and can even have no intersection with R_k (it can be totally on the other side, inside R_l).

This algorithm is similar to the one in [PMP14], that shares the same global structure (and the same restriction that a cell should not traverse a region), with the two steps to recover the missing edges in the Delaunay graph. The main difference is in Step (4): instead of considering the cells, their method is based on the vertices, that should satisfy the empty ball property. The vertex common

to cells $\mathcal{V}_i^\mathcal{E}, \mathcal{V}_j^\mathcal{E}, \mathcal{V}_k^\mathcal{E}$ is a Voronoi vertex if the circumscribed ball to the triangle (i, j, k) does not contain any point of \mathbf{x}_i . Hence, the points $\mathbf{x}_i, \mathbf{x}_j, \mathbf{x}_k$ are sent to the regions that have a non-empty intersection with the ball (in 3D, there are 4 cells meeting at a vertex, and it is the circumscribed ball to a tetrahedron). Infinite cells require a special treatment, and consider the cone defined by the edges (triangles in 3D) on the border of the Delaunay graph. On the one hand, computations are simpler than in our algorithm that needs computing Voronoi cells explicitly. On the other hand, the objects considered for sending a point \mathbf{x}_i to the neighboring cells are larger than in our case. In our case, the cost of sending more point than necessary is larger than the cost of computing the cells. Moreover, in our cosmological application shown in the next section, we can have a huge variation of pointset density, potentially creating pencil-shaped Voronoi cells on the border. Hence it is important to be able to determine which elements of the region boundary they encroach in order to avoid sending the point to too many nodes.

3 Large-scale optimal transport for cosmology

In this section, I shall present some early results, in a context of a practical application: some applications in computational physics require scalable optimal transport solvers. I shall first give a short overview on optimal transport and its application in physics, then present some results in early Universe reconstruction.

3.1 An example in early Universe reconstruction

We shall now see how the algorithm behaves in a practical scenario, in Early Universe Reconstruction. Figure 4-A shows the result of a cosmological simulation of structure formation, in a cube of 300 Mpc/h⁶ edge length. The figure shows a thin slice (5 Mpc/h thick) of the cube. Each point corresponds to a galaxy cluster. The goal of cosmological reconstruction [FMMS02, BFH⁺03, LMv21, vLM22, NSLM22] is to trace the trajectories of these galaxy clusters back in time, supposing that they started from a uniform initial condition. Under some simplifying assumptions (convexity of the integrated potential), it can be restated as a semi-discrete optimal transport problem. The goal, in the future, is to be able to apply such optimal-transport-based reconstruction to massive pointsets, with billions particles. When reconstructing from observational data, such gigantic-scale problems appear when modeling the unobserved dark matter as additional particles [NSLM22]. They are also needed in cosmological simulation of modified gravity [LBM24]. Typically, for our cube of 300 Mpc/h, it would be interesting to be able to solve optimal-transport problems with 2560³ points, which would give sufficient resolution to track fine-scaled dynamics. The

⁶300 mega parsecs, where the large-scale structure of the Universe starts to be homogeneous. For reference, the nearest star is 1.399 parsecs away from the sun, and the radius of the observable Universe is around 14.25 giga parsecs.

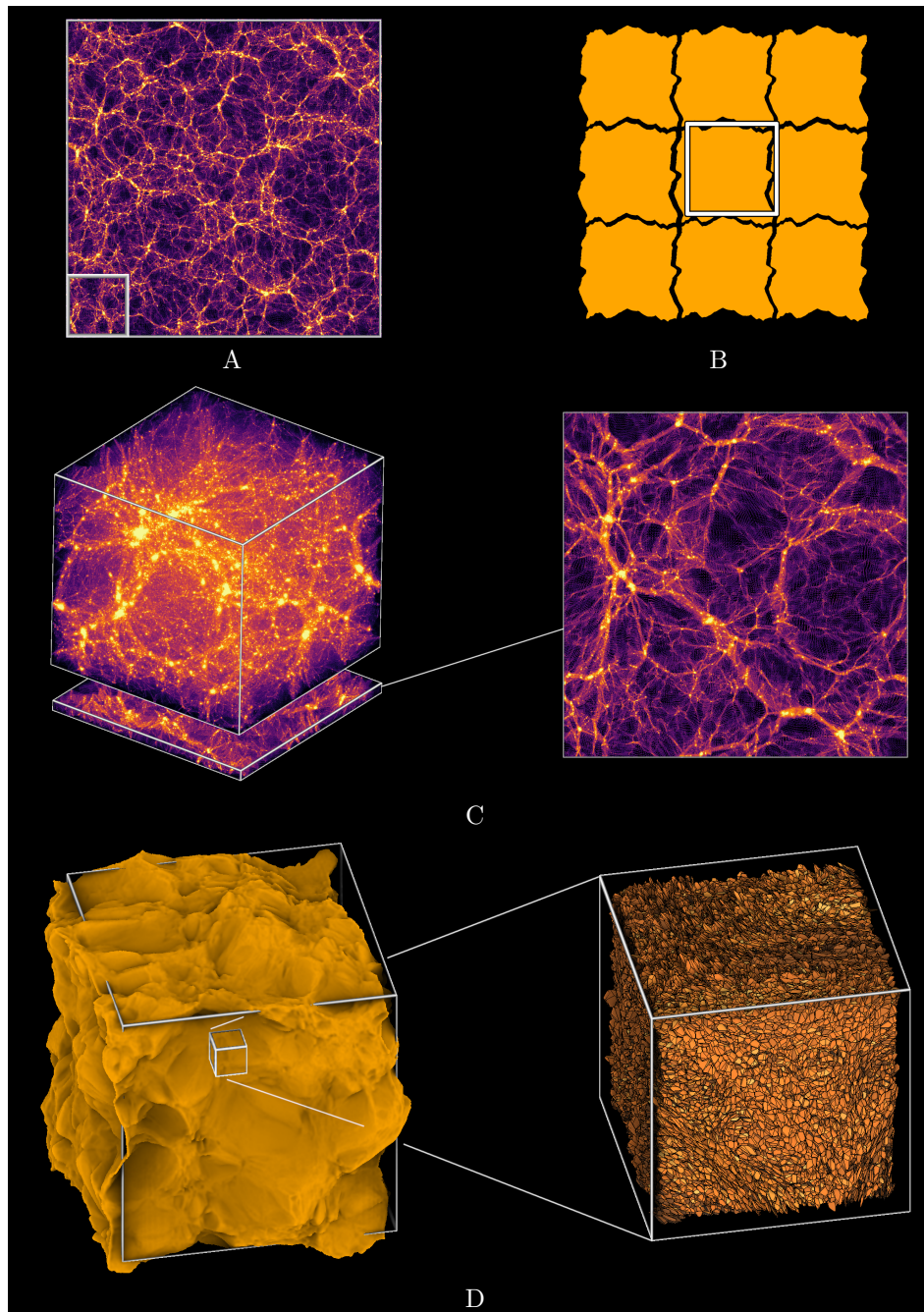


Figure 4: A: Thin-slice in a cosmological simulation of a 300 Mpc/h cube. Ultimately, the goal will be to compute optimal transport with 10 billion points. The cube will be decomposed into $5 \times 5 \times 5$ subvolumes (one of them highlighted). For now, the algorithm is tested and analyzed with periodic boundary conditions (B) in one of the subvolumes (C) with 100 million points. The reconstructed initial condition (D).

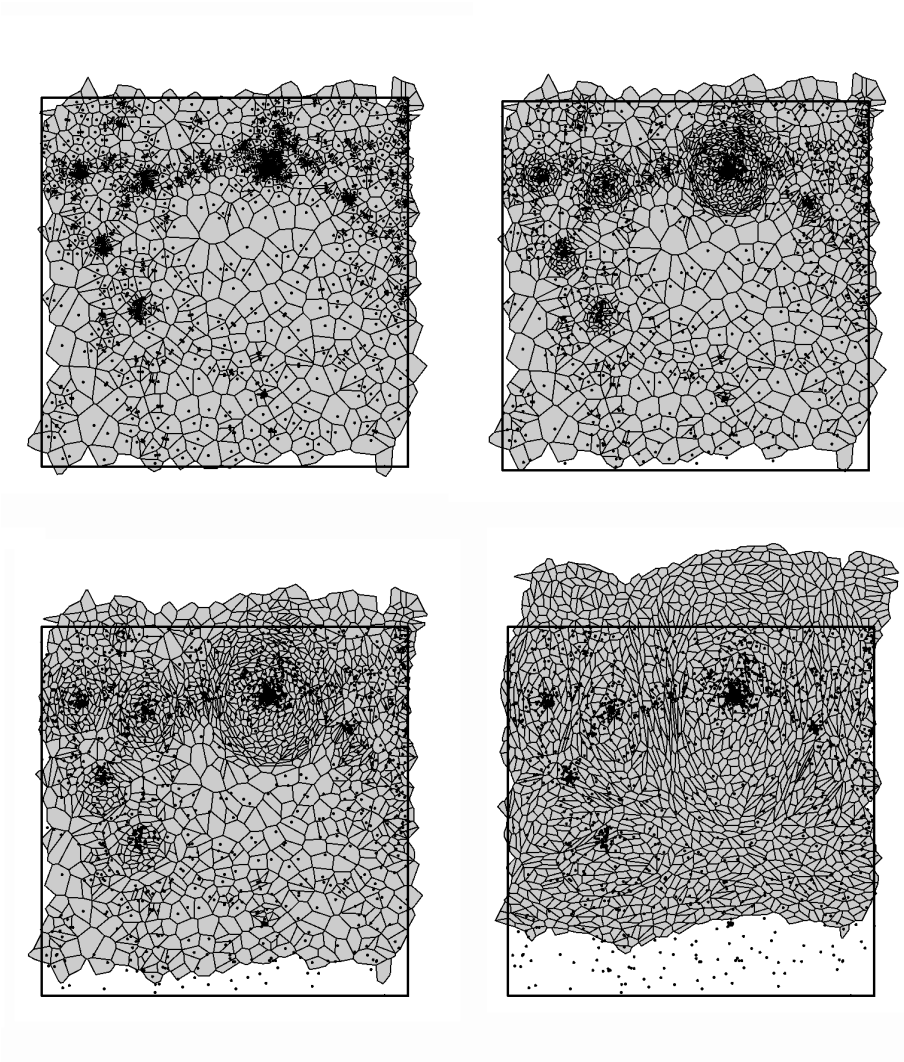


Figure 5: Newton iterations of semi-discrete optimal transport with periodic boundary conditions

idea will be to run the Distributed Voronoi Diagram on a PC cluster with 125 machines, each machine will be responsible for a cube of 60 Mpc/h with 100 million particles (512^3), depicted as a small square in the corner of Figure 4-A. Such a large-scale experiment will be the subject of later work. For now, I conducted a "proof-of-concept" experiment: as often done in cosmology and material science, to simulate a large volume of a globally homogeneous medium, one can use periodic boundary conditions. For instance, one could imagine considering the small cube in Figure 4 and connect its opposite faces before reconstructing the motion of the galaxy clusters. One then obtains an initial condition that paves the space, as the 2D example shown in Figure 4-B.

Figure 4-C shows the final timestep of a cosmological simulation, with 100 million points, in a cube of 60 Mpc/h edge length (same size of the small cube in Figure 4-A) with a periodic boundary condition. I made this simulation with a slightly modified version of [CTP94] (modifications are to make it work with 512^3 points, original version was limited to 256^3). Starting from this pointset, one can reconstruct the initial condition using optimal transport. In the end, one obtains a reconstructed initial condition that paves the 3D space, represented by a Laguerre diagram (Figure 4-D), and each Laguerre cells correspond to the matter that lumped to form one of the galaxy clusters. The closeup in Figure 4-D shows what these Laguerre cells look like in the central region of the cube.

Computing Voronoi and Laguerre diagrams with periodic boundary conditions is just a particular case of the algorithm presented in this article. In a 2D version, one considers 9 regions, indexed by "translation vectors" with coefficients in $\{-1, 0, 1\}$:

$$\begin{array}{c|c|c} R_{-1,1} & R_{0,1} & R_{1,1} \\ \hline R_{-1,0} & R_{0,0} & R_{1,0} \\ \hline R_{-1,-1} & R_{0,-1} & R_{1,-1} \end{array}$$

In practice, only $R_{0,0}$ is stored. In steps (4) and (10) of Algorithm 5, it "sends points to itself", by creating new copies of the points, translated according to which facet/edge/corner of the unit cube was traversed.

The example shown in Figure 4-C,D is a good "stress test" for semi-discrete optimal transport. Besides the number of points that starts to be large, and the additional difficulty of the periodic boundary conditions, this optimal transport problem is especially challenging, because at this small scale (relative to the size of the visible Universe), the variations of density are considerable: distances between the points vary by 5 orders of magnitude. Some regions are very dense, and some regions are nearly empty. This has several consequences for the iterative algorithm that computes the Laguerre diagram. As shown in the 2D example in Figure 5, it starts with a Voronoi diagram, then evolves the weights of a Laguerre diagram to find the (unique) Laguerre diagram such that the areas of the Laguerre cells match the masses of the points. As can be seen, the large variations of points density makes the first iterations quite "explosive". Then, as one can see, the Laguerre cells "travel" in space, to reach the position where the matter that corresponds to each cluster started from. As one can

Iter.	phase I				phase II			total t
	npts cross	npts out	t_{class}	t_{insert}	npts	t_{class}	t_{insert}	
0	653304	0	128	157	214709	8	68	585
1	646894	1	132	155	214702	8	7	498
2	648152	455	128	10	214356	7	4	337
3	650367	2577	127	11	213940	7	4	347
4	653716	7630	128	10	213606	7	4	350
5	656421	12349	129	11	213638	7	4	338
6	665380	33000	131	12	213970	8	4	363
7	679059	73802	127	12	214904	8	4	340
8	698289	154144	132	14	216874	8	4	347
9	727710	293819	130	15	220116	8	4	343
10	771755	529536	131	20	226543	9	4	363
11	800271	706303	133	23	232258	10	4	372
12	847297	1056938	132	27	244436	11	4	363
13	880521	1372424	136	32	255618	12	4	385
14	924347	1953509	134	37	276446	15	5	385
15	954754	2456543	137	44	294037	16	5	396
16	980676	2920710	139	52	308389	17	5	405
17	1025627	3811557	139	61	332190	21	5	425
18	1058683	4620154	141	73	351019	23	5	438
19	1129901	6152337	145	96	382185	28	6	492
20	1189443	7489788	147	115	404901	33	6	508
21	1234696	8662560	149	134	423503	39	7	552
22	1266823	9689720	150	143	438953	40	7	543
23	1322086	11475407	155	172	466236	51	7	604
24	1359869	12815746	158	182	486680	57	8	622
25	1410406	14844585	157	207	519654	62	8	655
26	1410606	14852765	155	209	519815	64	9	646
27	1412570	14983600	160	221	522130	65	9	1227
28	1420549	15472524	153	213	530152	68	9	1184
29	1431428	16207502	159	223	544584	73	10	721
30	1443134	16952680	163	236	562270	74	10	1262
31	1443904	16962972	159	243	562974	73	10	1192
32	1443921	16963014	165	263	563029	74	13	1294
33	1443921	16963014	165	250	563029	77	12	1429
34	1443921	16963014	163	255	563029	76	13	1327

Table 1: Statistics of the Laguerre diagram computations during the Newton iterations of a semi-discrete optimal transport problem with periodic boundary conditions. All times are in s.

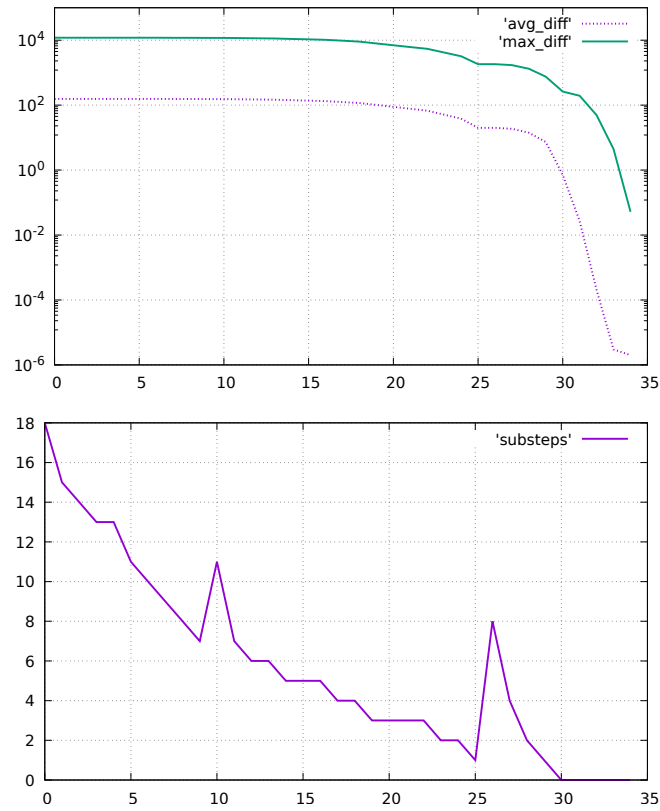


Figure 6: Top panel: Average cell difference and worst cell difference in function of Newton iterations (in percent of target cell measure, logarithmic scale). Bottom panel: number of substeps in each Newton iteration.

see, a Laguerre cell does not necessarily contain its site (unlike Voronoi cells). Another consequence of the high variations of density is that the matter that lumped to form the structures traveled a lot (up to 15% of cube edge length). In terms of our algorithm, it means that a significant number of points will be sent through the boundaries of the domain. The same behavior is expected when we will be running the algorithm on a cluster grid, with different pointsets in each cube.

In Table 1, I report different timings and statistics on Algorithm 5 executed in the context of semi-discrete optimal transport for early Universe reconstruction, with the pointset shown in Figure 4-B. The algorithm converged after 34 Newton iterations, which took 17h in total⁷. For each iteration, the table reports the number of points with a Laguerre cell that crosses the boundary of the domain (npts cross), the number of points completely on the other side of the boundary (npts out), the time to classify the points (t_{class}), to insert the points into the triangulation (t_{insert}), for both phases of the algorithm, as well as the total time for computing the Laguerre diagram (this includes the time to compute the initial triangulation in $R_{0,0,0}$). As can be seen, each iteration takes longer and longer, which is because the Laguerre cells travel a longer and longer distance (like in Figure 5), and a larger and larger number of points needs to be sent. Phase II takes a shorter time as compared to Phase I, because it is a purely combinatorial operation, whereas Phase I needs to compute the Laguerre cells and their relations with the boundary. However, execution time remains reasonable, even in the last iterations, that need to send more than 10% of the points. Figure 6 shows the convergence and the number of KMT substeps used by each Newton iteration. The average difference between a cell’s measure $|\text{Lag}_i^w|$ and the target measure ν_i (expressed in % of target cell measure), as well as the maximum difference in function of the iteration are both displayed. As can be seen, the first Newton iterations are challenged by the huge difference of density, and use a tiny $\alpha = 2^{-18}$ descent parameter. Starting from the 30th iteration, the algorithm enters a regime with quadratic speed of convergence, and the measure error of the worst cell quickly decreases.

4 Conclusions and future works

The numerical experiments presented here are a ”proof of concept”: this ”mock-up” numerical experiment tends to prove the feasibility of the approach for the targeted large-scale experiment evoked in Figure 4-A: the distributed Voronoi diagram algorithm exchanges a larger and larger number of points as Laguerre cells travel through the boundaries of the periodic domain. In the large-scale scenario, a similar number of points will be exchanged (but this time, with neighboring cluster nodes instead of the same cube seen from periodic boundaries). The experiment tends also to show that the algorithm resists the huge

⁷it can be probably brought back to 10h or less with sufficient RAM because my 100 GB machine was swapping a bit. Timings on a larger machine will be provided in future works.

variations of density, that challenge both its geometric part (Laguerre diagram) and numeric part (linear systems).

The software prototype is useful "as-is" for optimal-transport reconstruction with periodic boundary conditions, and was successfully applied it to problems with sizes ranging from 16M to 300M points [LMv21, vLM22, NSLM22, NPL⁺23]. Now the goal is to scale-up to problems of 1 billion points and above. This will make it possible to work with a volume of 300 Mpc/h (Figure 4-A) with the same resolution, and better measure different phenomena at a fine scale. This means running a cube of $5 \times 5 \times 5$ interconnected instances of the 60 Mpc/h reconstruction shown here on a cluster, which will be done in future works. Besides the implementation of the DVD algorithm on a cluster, this will also require a distributed linear solver (see [PSY⁺15] and references herein).

5 Acknowledgements

I wish to thank Nicolas Ray, Quentin Mérigot, Roya Mohayaee and Rémi Flamarly for many discussions.

References

- [Aur91] Franz Aurenhammer. Voronoi diagrams—a survey of a fundamental geometric data structure. *ACM Comput. Surv.*, 23(3):345–405, sep 1991.
- [BAR⁺21] Justine Basselin, Laurent Alonso, Nicolas Ray, Dmitry Sokolov, Sylvain Lefebvre, and Bruno Lévy. Restricted power diagrams on the GPU. *Comput. Graph. Forum*, 40(2):1–12, 2021.
- [BB00] Jean-David Benamou and Yann Brenier. A computational fluid mechanics solution to the monge-kantorovich mass transfer problem. *Numerische Mathematik*, 84(3):375–393, 2000.
- [BC13] Lorenzo Brasco and Guillaume Carlier. Congested traffic equilibria and degenerate anisotropic pdes. *Dyn. Games Appl.*, 3(4):508–522, 2013.
- [BCMO16] Jean-David Benamou, Guillaume Carlier, Quentin Mérigot, and Édouard Oudet. Discretization of functionals involving the monge-ampère operator. *Numerische Mathematik*, 134(3):611–636, 2016.
- [BFH⁺03] Y. Brenier, U. Frisch, M. Hénon, G. Loeper, S. Matarrese, R. Mohayaee, and A. Sobolevskii. Reconstruction of the early universe as a convex optimization problem. *Mon. Not. R. Astron. Soc.*, 346(501), 2003.
- [Bow81] Adrian Bowyer. Computing dirichlet tessellations. *Comput. J.*, 24(2):162–166, 1981.

- [Bre91] Yann Brenier. Polar factorization and monotone rearrangement of vector-valued functions. *Communications on Pure and Applied Mathematics*, 44:375–417, 1991.
- [Bre15] Yann Brenier. A double large deviation principle for monge-ampère gravitation. working paper or preprint, March 2015.
- [BY98] Jean-Daniel Boissonnat and Mariette Yvinec. *Algorithmic geometry*. Cambridge University Press, 1998.
- [CMYB19] Laurent Caraffa, Pooran Memari, Murat Yirci, and Mathieu Brédif. Tile & merge: Distributed delaunay triangulations for cloud computing. In Chaitanya K. Baru, Jun Huan, Latifur Khan, Xiaohua Hu, Ronay Ak, Yuanyuan Tian, Roger S. Barga, Carlo Zaniolo, Kisung Lee, and Yanfang (Fanny) Ye, editors, *2019 IEEE International Conference on Big Data (IEEE BigData), Los Angeles, CA, USA, December 9-12, 2019*, pages 1613–1618. IEEE, 2019.
- [CP84] M. Cullen and R. Purser. An extended lagrangian theory of semi-geostrophic frontogenesis. *J. of the Atmospheric Sciences*, pages 1477–1497, 1984.
- [CTP94] Hugh M. P. Couchman, Peter A Thomas, and Frazer R. Pearce. Hydra: An adaptive-mesh implementation of ppm-sph. *arXiv: Astrophysics*, 1994.
- [Cut13] Marco Cuturi. Sinkhorn distances: Lightspeed computation of optimal transport. In C.J. Burges, L. Bottou, M. Welling, Z. Ghahramani, and K.Q. Weinberger, editors, *Advances in Neural Information Processing Systems*, volume 26. Curran Associates, Inc., 2013.
- [Dem19] D. Demidov. Amgcl: An efficient, flexible, and extensible algebraic multigrid implementation. *Lobachevskii J. of Math.*, 40(5):535–546, May 2019.
- [dGWH⁺15] Fernando de Goes, Corentin Wallez, Jin Huang, Dmitry Pavlov, and Mathieu Desbrun. Power particles: an incompressible fluid solver based on power diagrams. *ACM Trans. Graph.*, 34(4):50:1–50:11, 2015.
- [EM90] Herbert Edelsbrunner and Ernst Peter Mücke. Simulation of simplicity: A technique to cope with degenerate cases in geometric algorithms. *ACM Trans. Graph.*, 9(1):66–104, jan 1990.
- [FMMS02] U. Frisch, S. Matarrese, R. Mohayaee, and A. Sobolevskii. A reconstruction of the initial conditions of the universe by optimal mass transportation. *Nature*, 417(260), 2002.

- [GM18] Thomas O. Gallouët and Quentin Mérigot. A lagrangian scheme à la brenier for the incompressible euler equations. *Found. Comput. Math.*, 18(4):835–865, 2018.
- [ILSS06] Martin Isenburg, Yuanxin Liu, Jonathan Richard Shewchuk, and Jack Snoeyink. Streaming computation of delaunay triangulations. *ACM Trans. Graph.*, 25(3):1049–1056, 2006.
- [Inr23] Inria. Geogram: a programming library of geometric algorithms. <http://https://github.com/BrunoLevy/geogram>, 2014-2023.
- [JKO98] Richard Jordan, David Kinderlehrer, and Felix Otto. The variational formulation of the fokker–planck equation. *SIAM Journal on Mathematical Analysis*, 29(1):1–17, 1998.
- [KMT19] Jun Kitagawa, Quentin Mérigot, and Boris Thibert. Convergence of a newton algorithm for semi-discrete optimal transport. *J. Eur. Math. Soc.*, 21(9), 2019.
- [L22] Bruno Lévy. Partial optimal transport for a constant-volume lagrangian mesh with free boundaries. *J. Comput. Phys.*, 451(C), feb 2022.
- [LB12] Bruno Lévy and Nicolas Bonneel. Variational anisotropic surface meshing with voronoi parallel linear enumeration. In Xiangmin Jiao and Jean-Christophe Weill, editors, *Proceedings of the 21st International Meshing Roundtable, IMR 2012, October 7-10, 2012, San Jose, CA, USA*, pages 349–366. Springer, 2012.
- [LBM24] Bruno Lévy, Yann Brenier, and Roya Mohayaee. Monge ampère gravity: from the large deviation principle to cosmological simulations through optimal transport, 2024.
- [Lév15] Bruno Lévy. A numerical algorithm for L_2 semi-discrete optimal transport in 3d. *ESAIM M2AN (Mathematical Modeling and Analysis)*, 2015.
- [Lév16] Bruno Lévy. Robustness and efficiency of geometric programs: The predicate construction kit (PCK). *Comput. Aided Des.*, 72:3–12, 2016.
- [Lév22] Bruno Lévy. Partial optimal transport for a constant-volume lagrangian mesh with free boundaries. *J. Comput. Phys.*, 451:110838, 2022.
- [LMSS20] Hugo Leclerc, Quentin Mérigot, Filippo Santambrogio, and Federico Stra. Lagrangian discretization of crowd motion and linear diffusion. *SIAM J. Numer. Anal.*, 58(4):2093–2118, 2020.

- [LMv21] Bruno Levy, Roya Mohayaee, and Sebastian von Hausegger. A fast semidiscrete optimal transport algorithm for a unique reconstruction of the early Universe. *Monthly Notices of the Royal Astronomical Society*, 506(1):1165–1185, 06 2021.
- [LS18] Bruno Lévy and Erica L. Schwindt. Notions of optimal transport theory and how to implement them on a computer. *Comput. Graph.*, 72:135–148, 2018.
- [Mér11] Quentin Mérigot. A multiscale approach to optimal transport. *Comput. Graph. Forum*, 30(5):1583–1592, 2011.
- [MFF⁺17] Rahul Mourya, André Ferrari, Rémi Flamary, Pascal Bianchi, and Cédric Richard. Distributed deblurring of large images of wide field-of-view, 2017.
- [Mon84] Gaspard Monge. Mémoire sur la théorie des déblais et des remblais. *Histoire de l’Académie Royale des Sciences (1781)*, pages 666–704, 1784.
- [MS24] Ismael Medina and Bernhard Schmitzer. Flow updates for domain decomposition of entropic optimal transport, 2024.
- [MT20] Quentin Mérigot and Boris Thibert. Optimal transport: discretization and algorithms. *CoRR*, abs/2003.00855, 2020.
- [NPL⁺23] Farnik Nikakhtar, Nikhil Padmanabhan, Bruno Lévy, Ravi K. Sheth, and Roya Mohayaee. Optimal transport reconstruction of biased tracers in redshift space. *Phys. Rev. D*, 108:083534, Oct 2023.
- [NSLM22] Farnik Nikakhtar, Ravi K. Sheth, Bruno Lévy, and Roya Mohayaee. Optimal Transport Reconstruction of Baryon Acoustic Oscillations. *Phys. Rev. Lett.*, 129(25):251101, December 2022.
- [OBSC00] Atsuyuki Okabe, Barry Boots, Kokichi Sugihara, and Sung Nok Chiu. *Spatial Tessellations: Concepts and Applications of Voronoi Diagrams*. Series in Probability and Statistics. John Wiley and Sons, Inc., 2nd ed. edition, 2000.
- [PC19] Gabriel Peyré and Marco Cuturi. Computational optimal transport. *Found. Trends Mach. Learn.*, 11(5-6):355–607, 2019.
- [PMP14] Tom Peterka, Dmitriy Morozov, and Carolyn Phillips. High-performance computation of distributed-memory parallel 3d voronoi and delaunay tessellation. In *SC ’14: Proceedings of the International Conference for High Performance Computing, Networking, Storage and Analysis*, pages 997–1007, 2014.

- [PSY⁺15] Jongsoo Park, Mikhail Smelyanskiy, Ulrike Meier Yang, Dheevatsa Mudigere, and Pradeep Dubey. High-performance algebraic multi-grid solver optimized for multi-core based distributed parallel systems. SC '15, New York, NY, USA, 2015. Association for Computing Machinery.
- [QLdGJ22] Ziyin Qu, Minchen Li, Fernando de Goes, and Chenfanfu Jiang. The power particle-in-cell method. *ACM Trans. Graph.*, 41(4):118:1–118:13, 2022.
- [RSL18] Nicolas Ray, Dmitry Sokolov, Sylvain Lefebvre, and Bruno Lévy. Meshless voronoi on the GPU. *ACM Trans. Graph.*, 37(6):265, 2018.
- [San15] Filippo Santambrogio. Optimal transport for applied mathematicians. *Birkhäuser, NY*, 55(58-63):94, 2015.
- [She97] Jonathan Richard Shewchuk. Adaptive Precision Floating-Point Arithmetic and Fast Robust Geometric Predicates. *Discrete & Computational Geometry*, 18(3):305–363, October 1997.
- [She05] Richard Shewchuk. Star splaying: an algorithm for repairing delaunay triangulations and convex hulls. In *Proceedings of the Twenty-First Annual Symposium on Computational Geometry*, SCG '05, page 237–246, New York, NY, USA, 2005. Association for Computing Machinery.
- [Slo87] S.W. Sloan. A fast algorithm for constructing delaunay triangulations in the plane. *Advances in Engineering Software (1978)*, 9(1):34–55, 1987.
- [Spr10] Volker Springel. E pur si muove: Galilean-invariant cosmological hydrodynamical simulations on a moving mesh. *Monthly Notices of the Royal Astronomical Society*, 401(2):791–851, 01 2010.
- [The23] The CGAL Project. *CGAL User and Reference Manual*. CGAL Editorial Board, 5.6 edition, 2023.
- [Vil03] Cédric Villani. *Topics in optimal transportation*. Graduate studies in mathematics. American Mathematical Society, Providence (R.I.), 2003.
- [Vil09] Cédric Villani. *Optimal transport : old and new*. Grundlehren der mathematischen Wissenschaften. Springer, Berlin, 2009.
- [vLM22] Sebastian von Hausegger, Bruno Lévy, and Roya Mohayaee. Accurate Baryon Acoustic Oscillations Reconstruction via Semidiscrete Optimal Transport. *Phys. Rev. Lett.*, 128(20):201302, May 2022.

- [Wat81] David Watson. Computing the n-dimensional delaunay tessellation with application to voronoi polytopes. *Comput. J.*, 24(2):167–172, 1981.